Sparse Reconstruction of the Ionosphere in the Equatorial Anomaly Region During the Solar Eclipse Based on Beidou Ground Based Augmentation System

Yun Sui[1,4(✉)], Haiyang Fu[1,4(✉)], Denghui Wang[2,3], Shaojun Feng[2,3], Feng Xu[1,4], and Yaqiu Jin[1,4]

[1] Key Laboratory for Information Science of Electromagnetic Waves (MoE), Fudan University, Shanghai 200433, China
{ysui18,haiyang_fu}@fudan.edu.cn
[2] Qianxun Spatial Intelligence (Zhejiang) Inc., Deqing 313200, Zhejiang, China
[3] Qianxun Spatial Intelligence Inc., Shanghai 200438, China
[4] Shanghai Innovation Center for BeiDou Intelligent Application, Shanghai 200433, China

Abstract. Computerized Ionospheric Tomography (CIT) is a technique to reconsruct the ionosphere based on the slant total electron content (STEC) on the path between satellites and stations. It is of great significance for the study of the temporal and spatial characteristics of the ionosphere and the monitoring of abnormal characteristics. The solar eclipse that occurred on June 21, 2020 provides an opportunity to study the impact of the solar eclipse on the ionosphere in the equatorial anomaly region, and provides an opportunity for further research on the impact of ionospheric changes on high-precision positioning. This paper uses data from the Beidou Ground Based Augmentation System (BDGBAS) and some overseas IGS stations to study the impact of the solar eclipse on the ionosphere in the low-latitude equatorial ionization anomaly (EIA) region. In order to better deal with the problems of sparse observations and uneven distribution, a tomographic sparse imaging method driven by compressed sensing fusion data-driven method was used to realize the three-dimensional electron density in EIA region under solar eclipse and non-eclipse states. The results show that there is a significant decrease in electron density and TEC during a solar eclipse compared to a non-eclipse period. The most obvious electron density and TEC depletion occur in the EIA peak area, and the TEC value decreases as much as 6–10 TECUs, accounting for 30–40% of non-eclipse states. With the pass of the solar eclipse, the electron density and TEC decrease also tend to gradually increase and then decrease. In addition, it was observed that the electron density increased during the solar eclipse, leading to the enhancement of TEC in some EIA regions, which was consistent with the prediction results of other literature. Compressed sensing fusion data-driven tomography method plays an important role in the study of ionospheric disturbances caused by solar eclipses and the impact of ionospheric changes during solar eclipses on high-precision positioning. The ionospheric tomography model based on the BDGBAS is of great significance to the fields of accurate ionospheric monitoring and abnormal warning.

C. Yang and J. Xie (Eds.): *China Satellite Navigation Conference (CSNC 2021) Proceedings*, LNEE 773, pp. 140–149, 2021.
https://doi.org/10.1007/978-981-16-3142-9_13

Keywords: Ionosphere · Tomography · BDGBAS · Solar eclipse · Equatorial Ionization Anomaly

1 Introduction

The ionosphere is one of the main sources of errors in radio propagation, affecting the application of technologies such as communication, navigation and positioning. Travelling Ionospheric Disturbances (TID) is a manifestation of atmospheric gravity waves in the ionosphere, accompanied by extreme events such as magnetic storms, earthquakes and solar eclipses, which can lead to degradation of precise positioning applications. The study of the temporal and spatial characteristics of the ionosphere and the monitoring of its anomalous characteristics are helpful to learn the temporal and spatial evolution of the ionosphere, and then realize the ionospheric error compensation in high-precision navigation and positioning. Currently, ionospheric detection methods include digital altimeter, high-frequency Doppler, beacon satellite Faraday rotation, and global positioning satellite system (GNSS). With the rapid development of GNSS, the Total Electron Content (TEC) calculated based on dual-frequency GPS observation data has been used as the main method of ionospheric detection. However, the spatial distribution of ionospheric TEC can only reflect the horizontal structure of the ionosphere, not its vertical structure.

Computerized ionospheric tomography (CIT) technology was first proposed by Austen et al. [1]. This method is based on the satellite and receiver path TEC to reconstruct the three-dimensional electron density distribution of the ionosphere [2]. A large number of studies have shown that CIT technology is suitable for monitoring the spatiotemporal distribution of large-scale ionospheric electron density and its disturbance [3, 4]. Many scholars have verified that CIT is an effective method for studying changes in ionospheric disturbances under magnetic storm conditions. Pajares et al. used ionospheric tomography technology to invert the global electron density distribution during a magnetic storm, and analyzed the changes in the electron density during a magnetic storm [5]. Yao et al. used CIT technology to invert the three-dimensional space-time distribution of ionospheric electron density in the European region during three different types of strong magnetic storms from 2003 to 2006 based on IGS tracking station data, and effectively analyzed the ionospheric disturbance during the occurrence of magnetic storms situation [6]. Chen et al. designed a CIT algorithm that combines the least squares method with constraints, and evaluated the performance of this method in detecting ionospheric electron density disturbances at a wavelength of about 200 km based on simulation experiments [7]. Bolmgren et al. used the North American Global Positioning System data and the Multi-Instrument Data Analysis Software (MIDAS) tomographic method to study the ionospheric disturbance caused by a strong geomagnetic storm in 2003 [8].

Equatorial Ionization Anomaly (EIA) phenomenon mainly refers to the formation of troughs at the equator by the plasma through the upward E × B drift [16]. CIT technology demonstrates powerful capabilities in the study of equatorial ionization anomalies. Muella used the MIDAS tomography algorithm to reconstruct the Brazilian equatorial

ionization anomaly region, and verified the accuracy of MIDAS electron density imaging during the geomagnetic quiet period [9]. Prol et al. developed a modified form of the MART tomography method, drawing a regional ionospheric tomography map of Brazil with equatorial anomalies [10].

During a solar eclipse, the ionosphere quickly experienced a process of gradual disappearance of the ionization source and then gradually returning to normal in a short period of time. A number of studies have shown that before and after the TEC decrease related to the solar eclipse, the large-scale travelling ionospheric disturbance (LSTID) activity has increased [11–13]. Coster et al. used GNSS data during the solar eclipse that occurred in the continental United States on August 21, 2017, to study the latitude and longitude response of TEC changes during the solar eclipse, and observed the existence of TID [11]. In order to study the solar eclipse that occurred on June 21, 2020, Zhang et al. used observations from ionosondes, Beidou Global Navigation Satellite System (GNNS) receivers, COSMIC2, DMSP and SWARM satellites to study the response of ionosphere to solar eclipse [12]. Huang et al. used ground and space observations, including the total electron content of the Beidou geostationary satellite, the two-dimensional TEC map of the globally dense global navigation satellite system receiver, the ionsonde, and the in-situ electron density (Ne) and SWARM and the electron temperature (Te) of the China Earthquake Electromagnetic Satellite, studied the response of the low-latitude ionosphere to this solar eclipse [13].

The trajectory of the solar eclipse on June 21, 2020 is unique. The maximum geographic latitude of the solar eclipse is about 30° north latitude. It provides an opportunity to study the impact of the solar eclipse on the ionosphere in the equatorial anomaly region, and provides an opportunity for further research on the impact of ionospheric changes on high-precision positioning. In this paper, using data from the Beidou Ground Based Augmentation System (BDGBAS) built by Qianxun Spatial Intelligence Inc. and some overseas IGS stations, the tomographic sparse imaging method by compressed sensing fusion data-driven is used to reconstruct the three-dimensional electron density in EIA area during the solar eclipse [14, 15]. Study the temporal and spatial evolution of the ionosphere during the occurrence of a solar eclipse based on the three-dimensional electron density.

2 Ionospheric Tomography Reconstruction Method

In order to solve the ill-posed problem, the previous tomographic work usually assumes that the ionosphere does not change within half an hour to two hours, thereby accumulating a large number of observations to achieve tomography, which is unreasonable [17–22]. The tomographic imaging method used in this research is the tomographic sparse imaging method based on compressed sensing fusion data-driven proposed in literature [14, 15].

1. Observation matrix building module

Receive the original observation data and navigation messages, calculate the satellite position and construct the ionospheric tomography model observation matrix ϕ_{total} according to the geometric relationship between the satellite and the station.

2. Differential part slant electron total content calculation module

The un-differenced and uncombined precision point positioning (UCPPP) algorithm is used to extract the slant ionospheric delay $I_k^{s'}$, which is related with the Slant Total Electron Content (STEC) integrated by the electron density N_e on the path between satellite s and receiver k [16].

$$I_k^{s'} = \frac{\mathrm{a} \cdot STEC_k^s}{f_1^2} + \frac{f_2^2}{f_1^2 - f_2^2} DCB_k - \frac{f_2^2}{f_1^2 - f_2^2} DCB^s \tag{1}$$

where 'a' represents the ionospheric propagation path integral constant 40.3, f_1 is the frequency of the first carrier, f_2 is the frequency of the second carrier, $STEC_k^s$ is the total electron content on the slant path between base station k and satellite s, and DCB_k is the hardware delay deviation of base station k, DCB^s is the hardware delay deviation of satellite s.

In order to eliminate the influence of the DCB_k in (1), inter-satellite differential processing is performed on the ionospheric delay. Select a reference star, calculate the difference between the ionospheric delay observations of each satellite and the reference star, the differential ionospheric delay $\mathrm{d}I_k^{s'}$ between station k and satellite s is expressed in the following way:

$$\mathrm{d}I_k^{s'} = I_k^{s'} - I_k^{ref'} = \frac{\mathrm{a} \cdot dSTEC_k^s}{f_1^2} - \frac{f_2^2}{f_1^2 - f_2^2}(DCB^s - DCB^{ref}) \tag{2}$$

After the DCB^s is eliminated by reading the external product, the total difference electron content between the station k and the satellite s is calculated and used as the input observation of the tomographic model:

$$dSTEC_k^s = \frac{f_1^2 \cdot \mathrm{d}I_k^s}{\mathrm{a}} \tag{3}$$

The NeQuick2 model is used to calculate the proportional relationship between the total electron content corresponding to the GNSS rays in the inversion area and the GNSS rays in the support area. According to the proportional relationship and the total difference electron content $dSTEC_k^s$ in (3), the differential Partial Slant Total Electron Content (dPSTEC) of the GNSS rays in the inversion area is calculated [15].

3. Projection matrix calculation module

Based on the NeQuick2 model, the historical data of the electron density in the inversion area is collected, and a data-driven algorithm is used to construct a projection matrix ψ that characterizes the characteristics of the ionosphere.

4. Differential part slant electron total content calculation module

According to the observation matrix ϕ_{total}, dPSTEC and projection matrix ψ, construct an objective function that adds L1 norm sparse regularization term.

$$\overline{w} = \arg\min_{w} \left\{ \| dPSTEC_{\mathrm{total}} - \phi_{\mathrm{total}} \cdot \psi \cdot w \|_2^2 + \lambda_{CS} \cdot \| w \|_1 \right\}. \tag{4}$$

where w is the quantity to be solved, ψ is the projection matrix that characterizes the ionosphere, and λ_{CS} is the hyperparameter that controls the proportion of error terms and sparse terms in the objective function. Use Bayesian optimizer to optimize λ_{CS}. The compressed sensing algorithm is used to solve the optimization problem to obtain the quantity w, thereby calculating the electron density.

3 Research Area and Data Source

An annular solar eclipse crossed from Africa to Southeast Asia and crossed the low-latitude ionosphere from UT03:51 to UT09:30 on June 21, 2020 and its trajectory is shown in Fig. 1 [13]. In this research, we used the Beidou Ground Based Augmentation System (BDGBAS) built by Qianxun Spatial Intelligence Inc. and some IGS stations, a total of 104 GNSS stations, to collect pseudorange observations and carrier phase observations, with an epoch interval of 30 s. Most of the stations are located in the middle and low latitudes corresponding to Asia and Australia. The distribution of these stations is very suitable for studying the influence of solar eclipse on the ionosphere in equatorial anomaly regions.

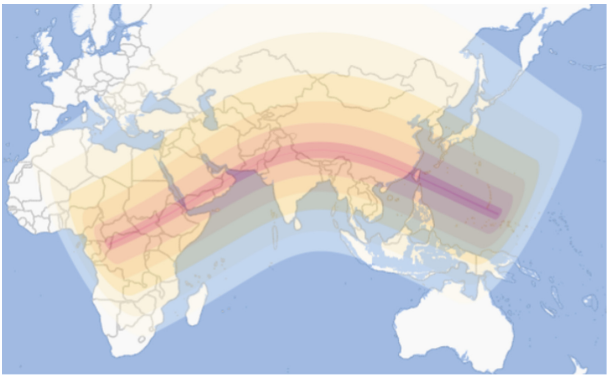

Fig. 1. The pass of the 21 June 2020 annular solar eclipse [24].

The selected 104 stations are still sparsely distributed relative to this area, resulting in insufficient observations. Therefore, the tomographic sparse imaging method based on compressed sensing fusion data-driven is used for June 21, 2020 (solar eclipse) and June 18, 2020 (non solar eclipse). Under the two states, the ionosphere in this area is tomographic. The ionospheric parameters to be inverted are as follows:

- Time: UT06:30–UT09:30, time resolution is 5 min, reconstruction interval is 30 min;
- Area to be retrieved: longitude range 100°–140°, latitude range −5°–35°, height range 80 km–1400 km;
- Grid: resolution of longitude* latitude is 2.5° * 2.5°; height uses variable resolution: 20 km in 80 km–1000 km, 100 km in 1000 km–1400 km;
- Cutoff elevation angle: 30°;

4 Results and Analysis

Figure 2 shows the Dst index from June 18 to 24, 2020. During the solar eclipse period on June 21, the solar activity is very low, and the geomagnetic index is around zero, so the geomagnetic activity is relatively quiet. In order to study the impact of the solar eclipse on the ionosphere in the low-latitude equatorial anomaly region, data from June 21, 2020 (solar eclipse) and June 18, 2020 (non-eclipse) UT6:30–UT9:30 are selected for ionospheric tomography reconstruction. The three-dimensional electron density distribution in the EIA area are shown in the left and middle columns of Fig. 3, respectively. It is observed that whether there is a solar eclipse or not, the equatorial anomaly appears in the area, that is, the electron density has a trough. Comparing the electron density in the two states of the solar eclipse and the non-eclipse, it is found that the electron density during the eclipse is significantly lower than that of the non-eclipse.

In order to further analyze the electron density changes caused by the solar eclipse, the difference between the electron density in the case of non-eclipse and solar eclipse is given in the right column of Fig. 3. There is a significant decrease in electron density during the solar eclipse, and the most obvious decrease in electron density occurs in the EIA peak area. This finding is consistent with the conclusion of the literature [13]. In addition, it was observed that during the solar eclipse between UT6:30 and UT:7:30, the electron density increases in the altitude of 200–300 km.

In order to more clearly characterize the changes of the ionosphere with latitude and longitude, the total electron content (TEC) is obtained by the vertical integration of the electron density, and the absolute value and the percentage of the TEC difference between the two states are calculated, respectively, as shown in the left and right columns of Fig. 4. The TEC changes obtained by the two calculation methods are very similar, and the TEC decrease is asymmetric in latitude. Similar to the electron density results, the most obvious TEC decrease occurs in the EIA peak area, and the maximum TEC attenuation reaches 6–10 TECUs, accounting for 30–40% of the non-eclipse state. In addition, it has been observed that during the solar eclipse, TEC enhancement occurs in some areas of the EIA within the range of longitude 110°–140°. This finding is consistent with the results predicted by Dang et al. in the simulation study of this eclipse [25], that is, the change in total electron content in the region is strongly affected by the neutral wind dynamics caused by the solar eclipse, which leads to the enhancement of TEC in

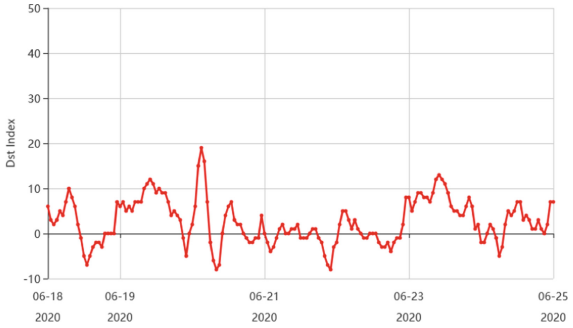

Fig. 2. The temporal variation of Dst index in June 2020 [25].

the EIA region during the solar eclipse. The maximum TEC enhancement observed this time is about 7.5 TECU, accounting for 20% of the non-eclipse state.

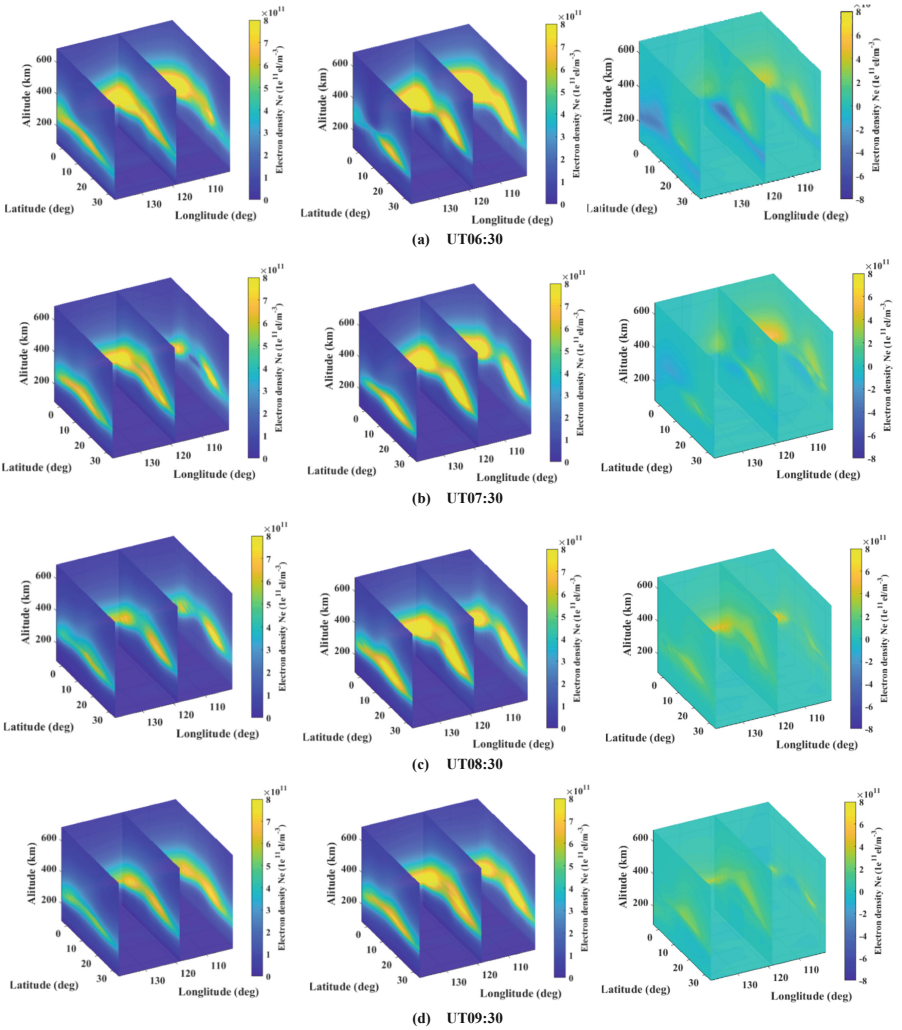

Fig. 3. Three-dimensional electron density distribution. Left column: ionospheric electron density on June 21, 2020 (solar eclipse); Middle column: ionospheric electron on June 18, 2020 (non solar eclipse); Right column: ionospheric electron density difference between non solar eclipse and solar eclipse.

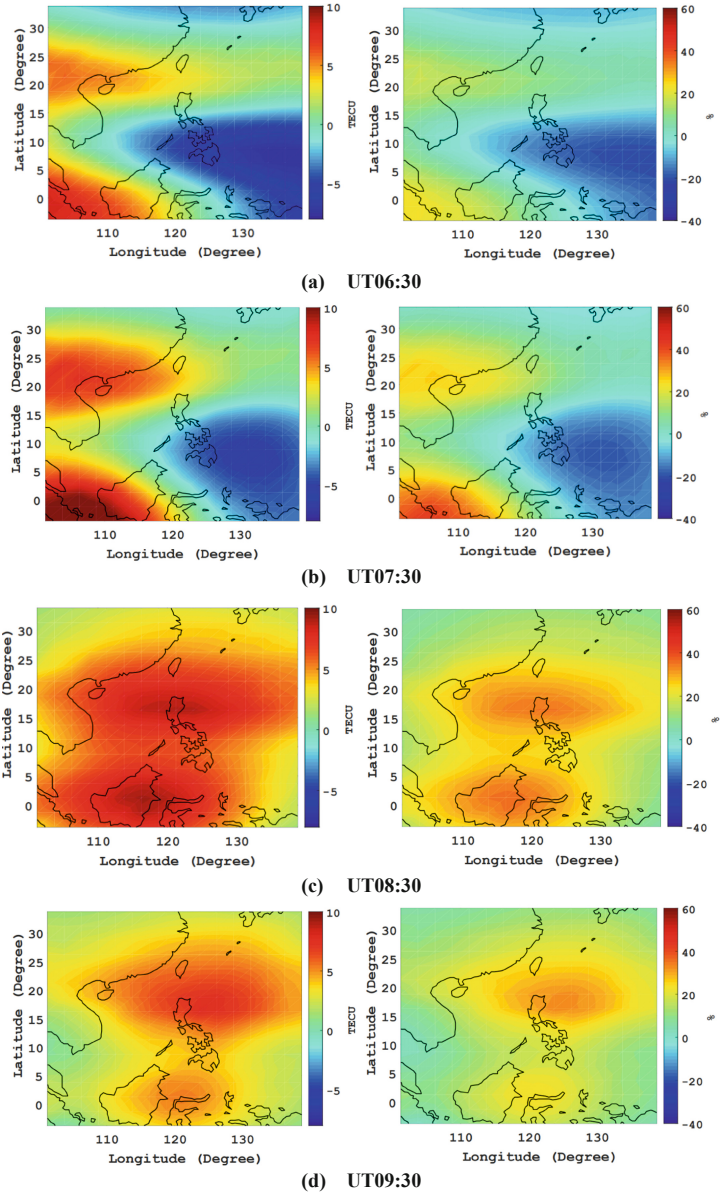

Fig. 4. The ionospheric VTEC difference between non solar eclipse and solar eclipse: Left column shows absolute difference in TECU; Right column shows the diffffference expressed as percentage of background TEC.

5 Conclusion and Discussion

This paper uses data from the Beidou Ground Based Augmentation System (BDGBAS) and some overseas IGS stations to study the impact of the solar eclipse on the ionosphere

in the low-latitude equatorial ionization anomaly (EIA) region. A tomographic sparse imaging method driven by compressed sensing fusion data-driven method was used to realize the three-dimensional electron density in EIA region under solar eclipse and non-eclipse states. Studies have shown that there is a significant decrease in electron density and TEC during solar eclipses compared to non-eclipse periods. The most obvious electron density and TEC attenuation occur in the EIA peak area. With the pass of the solar eclipse, the electron density and TEC attenuation also tend to gradually increase and then decrease. The TEC value drops up to 6–10 TECUs, accounting for 30–40% of the non-eclipse state. In addition, it was observed that during the solar eclipse, the electron density increased in the altitude range of 200–300 km, which led to the enhancement of TEC in some EIA areas.

In Addition, We Will Use This Tomographic Method to Study the Ionospheric Disturbance Caused by the Solar Eclipse, and the Impact of Ionospheric Changes on High-Precision Positioning. The Relevant Research Results Will Be Shown in Subsequent Papers. The Tomographic Sparse Imaging Method Based on Compressed Sensing Fusion Data-Driven Method Can Effectively Reconstruct the Three-Dimensional Electron Density of the Ionosphere by Relying on Sparse Observation, and Realize Real-Time Ionospheric Tomography. The Ionospheric Tomography Model Based on the BDGBAS is of Great Significance for Accurate Ionospheric Monitoring and Abnormal Warning.

Acknowledgement. This work is supported by the Shanghai Science and Technology Committee under Grant 19ZR1403900. Thank Lei Jiuhou and Liu Libo for the opportunity to participate in the Ziwu Engineering Seminar.

References

1. Austen, J.R., Franke, S.J., Liu, C.H., et al.: Application of computerized tomography techniques to ionospheric research. In: International Beacon Satellite Symposium on Radio Beacon Contribution to the Study of Ionization and Dynamics of the Ionosphere and to Corrections to Geodesy and Technical Workshop, vol. 1, pp. 25–35 (1986)
2. Wen, D.: GPS-based ionospheric tomography algorithm and its application research. Institute of Surveying and Geophysics, Chinese Academy of Sciences, Wuhan (2007)
3. Na, H., Lee, H.: Orthogonal decomposition technique for ionospheric tomography. Int. J. Imag. Syst. Technol. **3**(4), 354–365 (1991)
4. Raymund, T.D., Austen, J.R., Franke, S.J., Liu, C.H., Klobuchar, J.A., Stalker, J.: Application of computerized tomography to the investigation of ionospheric structures. Radio Sci. **25**(5), 771–789 (1990)
5. Hernández-Pajares, M., Juan, J.M., Sanz, J., et al.: Global observation of the ionospheric electronic response to solar events using ground and LEO GPS data. J. Geophys. Res. Space Phys. **103**(A9), 20789–20796 (1998)
6. Yibin, Y., Jiajun, C., Peng, C., et al.: Three-dimensional tomography and evolution analysis of the ionosphere in the European region during the magnetic storm from 2003 to 2006. J. Wuhan Univ. (Inf. Sci. Ed.) **39**(2), 132–136 (2014)
7. Chen, C.H., Saito, A., Lin, C.H., et al.: Medium-scale traveling ionospheric disturbances by three-dimensional ionospheric GPS tomography. Earth Planets Space **68**(1), 32 (2016)
8. Bolmgren, K., Mitchell, C., Jayawardena, T.P., et al.: Tomographic imaging of a large scale TID during the Halloween Storm of 2003. Ann. Geophys. Discuss. **2020**, 1–14 (2020)

9. Muella, M.T.A.H., De Paula, E.R., Mitchell, C.N., et al.: Tomographic imaging of the equatorial and low-latitude ionosphere over central-eastern Brazil. Earth Planets Space **63**(2), 129–138 (2011)
10. Prol, F.D.S., Camargo, P.D.O., Hernandez-Pajares, M., et al.: A new method for ionospheric tomography and its assessment by ionosonde electron density, GPS TEC, and single-frequency PPP. IEEE Trans. Geosci. Remote Sens. **57**(5), 2571–2582 (2018)
11. Coster, A.J., Goncharenko, L., Zhang, S.-R., et al.: GNSS observations of ionospheric variations during the 21 August 2017 solar eclipse. Geophys. Res. Lett. **44**(24), 12,041–12,048 (2017)
12. Zhang, R., Le, H., Li, W., et al.: Multiple technique observations of the ionospheric responses to the 21 June 2020 solar eclipse. J. Geophys. Res. Space Phys. **125**(12), e2020JA028450 (2020)
13. Huang, F., Li, Q., Shen, X., et al.: Ionospheric responses at low latitudes to the annular solar eclipse on 21 June 2020. J. Geophys. Res. Space Phys. **125**(10), e2020JA028483 (2020)
14. Sui, Y., et al.: Sparse reconstruction of regional ionospheric tomography based on Beidou ground based augmentation system. In: Sun, J., Yang, C., Xie, J. (eds.) China Satellite Navigation Conference (CSNC) 2020 Proceedings: Volume II. CSNC 2020. Lecture Notes in Electrical Engineering, vol. 651, pp. 673–683. Springer, Singapore (2020). https://doi.org/10.1007/978-981-15-3711-0_60
15. Sui, Y., Fu, H., Wang, D., et al.: Sparse reconstruction of 3D regional ionospheric tomography based on Beidou ground based augmentation system. IEEE Trans. Geosci. Remote Sens. (undergoing review)
16. Balan, N., Liu, L., et al.: A brief review of equatorial ionization anomaly and ionospheric irregularities. Earth Planet. Phys. **2**, 257–275 (2018)
17. Ma, X.F., Maruyama, T., Ma, G., et al.: Three-dimensional ionospheric tomography using observation data of GPS ground receivers and ionosonde by neural network. J. Geophys. Res. Space Phys. **110**(A5) (2005)
18. Garcia, R., Crespon, F.: Radio tomography of the ionosphere: analysis of an underdetermined ill-posed inverse problem and regional application. Radio Sci. **43**(2), 1–13 (2008)
19. Yavuz, E., Arikan, F., Arikan, O.: A hybrid reconstruction algorithm for computerized ionospheric tomography. In: Recent Advances in space Technologies, pp. 782–787. IEEE (2005)
20. Fougere, P.F.: Ionospheric radio tomography using maximum entropy 1. Theory and simulation studies. Radio Sci. **30**(2), 429–444 (1995)
21. Markkanen, M., et al.: Bayesian approach to satellite radio tomography with applications in the Scandinavian sector. Ann. Geophys. **13**, 1277–1287 (1995)
22. Hirooka, S., Hattori, K., Takeda, T.: Numerical validations of neuralnetwork-based ionospheric tomography for disturbed ionospheric conditions and sparse data. Radio Sci. **46**(5), 1–13 (Oct. 2011)
23. https://www.timeanddate.com/eclipse/map/2020-june-21
24. http://www.sepc.ac.cn/dstModel_chn.php
25. Dang, T., Lei, J., Wang, W., Yan, M., Ren, D., Huang, F.: Prediction of the thermospheric and ionospheric responses to the 21 June 2020 annular solar eclipse. Earth Planet. Phys. **4**(3), 231–237 (2020). https://doi.org/10.26464/epp2020032